Cell, Vol. 102, 615–623, September 1, 2000, Copyright ©2000 by Cell Press

Structure of Functionally Activated Small Ribosomal Subunit at 3.3 Å Resolution

Frank Schluenzen,*‖ Ante Tocilj,*‖ Raz Zarivach,† Joerg Harms,* Marco Gluehmann,* Daniela Janell,* Anat Bashan,† Heike Bartels,† Ilana Agmon,† François Franceschi,‡§ and Ada Yonath*†

*Max-Planck-Research Unit for Ribosomal Structure
22603 Hamburg
Germany
†Weizmann Institute
76100 Rehovot
Israel
‡Max-Planck-Institute for Molecular Genetics
14195 Berlin
Germany

Summary

The small ribosomal subunit performs the decoding of genetic information during translation. The structure of that from *Thermus thermophilus* shows that the decoding center, which positions mRNA and three tRNAs, is constructed entirely of RNA. The entrance to the mRNA channel will encircle the message when a latch-like contact closes and contributes to processivity and fidelity. Extended RNA helical elements that run longitudinally through the body transmit structural changes, correlating events at the particle's far end with the cycle of mRNA translocation at the decoding region. 96% of the nucleotides were traced and the main fold of all proteins was determined. The latter are either peripheral or appear to serve as linkers. Some may assist the directionality of translocation.

Introduction

Ribosomes are the universal ribonucleoprotein particles that translate the genetic code into proteins. They are built of two subunits, which associate upon initiation of protein synthesis. The large subunit (1.45 MDa in bacterial ribosomes) catalyzes the peptide bond formation and provides a path for the nascent polypeptide chain. The small subunit (0.85 MDa) initiates mRNA engagement, decodes the message, governs mRNA and tRNA translocation, and controls fidelity of codon–anticodon interactions.

Recent reports describe crystallographically determined low- and medium-resolution partial structures for the intact ribosome (70S) from *T. thermophilus,* at 7.8 Å (Cate et al., 1999), the large subunit from *Haloarcula marismortui,* at 5 Å (Ban et al., 1999), the small (30S) subunit from *T. thermophilus,* at 5.5 Å (Clemons et al., 1999), and the activated form of this subunit, at 4.5 Å (Tocilj et al., 1999). Advances in electron cryomicroscopy (cryo-EM) have also revealed new features of ribosomal particles and their complexes (Gabashvili et al., 1999b, 2000; Stark et al., 2000). In parallel, the structures of several ribosomal protein–RNA complexes have been determined at high resolution (Conn et al., 1999; Wimberly et al., 1999; Agalarov et al., 2000; Nikulin et al., 2000).

The small ribosomal subunit from *T. thermophilus* contains 19 proteins (Tsiboli et al., 1994), a small polypeptide of 26 amino acids, called Thx (Choli et al., 1993) and an RNA chain, called 16S, of 1518 nucleotides (Murzina et al., 1988). Base pairing and stacking interactions induce local folding of most of this long RNA chain, resulting in multiple junctions of helical regions, frequently interrupted by mismatches and internal bulges. The structure of the small subunit, presented here at 3.3 Å resolution (Figure 1), is an essentially complete molecular description. It includes 1457 nucleotides and most of the fold of all 19 proteins belonging to this particle. It shows known as well as newly detected folding and packing motifs. It provides insight into the decoding mechanism and its universality, and highlights the role of selected components in maintaining the sophisticated architecture of the ribosome.

Results and Discussion

Structure Determination

The 3.3 Å resolution map (Figure 1 and Table 1), obtained by multiple isomorphous replacement and anomalous scattering (MIRAS) is sufficiently clear that most of the structure could be traced. In many regions bases were well separated and purines and pyrimidines could be assigned. Likewise, many of the proteins loop and side chains could be identified. The ribosome is a molecular machine with multiple states, and particular segments are likely to be disordered in any one of these states. Although improvement is expected at higher resolution, we believe that most of the less well resolved map regions, accounting for less than 4% of all nucleotides, show that these RNA segments are indeed flexible.

Our structure contains most of the 16S nucleotides and all the proteins of the 30S subunit. Localization of the proteins was based on the large body of noncrystallographic information, as described in (Tocilj et al., 1999). We placed the structures of S4, S5, S6, S7, S8, S15, S17, S18, and S19, as determined by X-ray crystallography or NMR (Ramakrishnan and White, 1998; Helgstrand et al., 1999; Agalarov et al., 2000) and identified density that should account for most of the parts of these proteins that were not determined in isolation. We also identified parts of the known structures that seem to assume different conformations within the ribosome. In addition, we traced, fully or partially, proteins S2, S3, S9, S10, S11, S12, S13, S14, S16, and S20. As for the above, the positioning of these proteins was based on the available biochemical, biophysical, and functional data. We confirmed the positions of S11 and S13 by the independent localization of heavy-atom clusters that were bound to their exposed cysteines prior to crystallization (Weinstein et al., 1999).

§To whom correspondence should be addressed (e-mail: franceschi@molgen.mpg.de).
‖These authors contributed equally to the work.

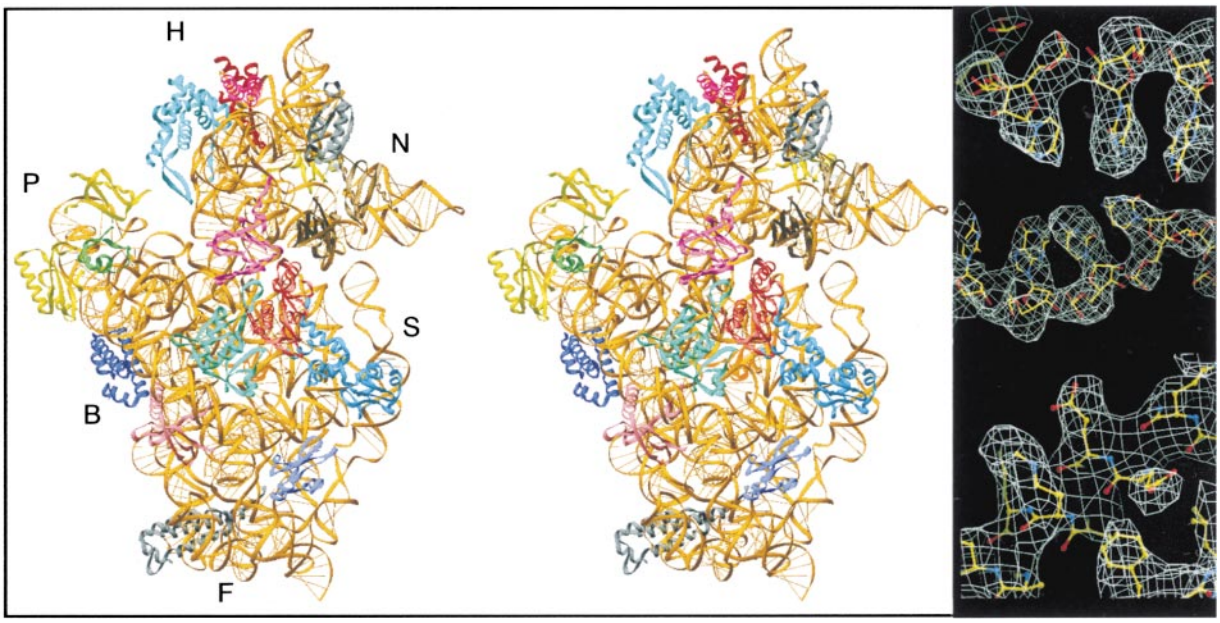

Figure 1. The Small Subunit and Its Electron Density Map

(Left and center) A stereo representation of the full model described in this paper. RNA is shown in gold, using a ribbon backbone and simple lines for base pairs. The differently colored helical segments and loops are the proteins. The major subdivisions are labeled: H, head; B, body; S, shoulder; P, platform; N, nose; F, foot.

In all figures, the head is at the top of the drawing and the foot at the bottom.

These portions of Figures 1–3 were made with Ribbons (Carson, 1997).

(Right) Segments showing RNA (top and middle pannels) and proteins (bottom) of the MIRAS map at 3.3 Å resolution, with the model superimposed. Made with O (Jones and Kjeldgaard, 1997).

Global Organization of the Small Subunit

The particle that emerges from our map (Figure 1) contains the morphological features familiar from cryo-EM reconstructions. The traditional subdivisions are the "head," "neck," and "body"; the body has a "shoulder," a "platform," and a "foot" with a "toe" (called also "spur"). The head has a "nose" with a further protuberance, the "beak."

Three long helices, called here "longitudinal" to designate their direction, H44, H7, and H16/H17 (Figure 2) run parallel to the long axis of the subunit (vertically in the view in Figure 1). Among them H44 and H16/H17 are located on the rather flat surface that faces the 50S subunit. The three longitudinal helices are linked by transverse features, placed like ladder rungs between them. Principal among these transverse helices are H21-H23 (Figure 2), which lie in an inclined lune extending from the shoulder to the platform. The head contains mainly short helices, in marked contrast to the long duplexes of the body. It has a bilobal architecture, with H34 serving as the bridge between hemispheres (Figure 2). The head joins the body through a single RNA helix, H28 which appears to act as a hinge. In addition, the upper part of the shoulder (H16/H18) and the lower part of the nose (H33/H34) form a noncovalent body–head connection (Figures 1 and 3). We refer to this interaction as the "latch." It surrounds the entrance to an elongated, curved channel, proposed by us to be the conduit for the mRNA chain, based on previous structural studies (Arad et al., 1987; Mueller et al., 1997; Cate et al., 1999).

All the major functional features of the subunit consist of RNA elements; the proteins appear to serve largely as struts, linkers, and supports. Of interest are long extensions of proteins which penetrate into rRNA regions, similar to those detected in the nucleosome (Luger et al., 1997). Some of them reach distal proteins. For example, protein S12 contains a long tail which spans the particle, extending toward S17 (Figure 2). Parts missing in the available crystallographic or NMR structures that were readily traced in our map are an α-helical region at the N terminus of S5, a β strand protruding from S7, and a short arm originating at S18 and pointing toward S6.

Only one protein, S12, is located at the RNA-rich surface that interacts with the large subunit. Two additional proteins, S7 and S15, that are located at the rims of the subunit interface region, are partially involved in tRNA binding or in intersubunit contacts, respectively. A few proteins, such as S4, S5, S8, and S12 may contribute to the fidelity and the directionality of the translocation (see below). About half a dozen are peripheral, located on the particle's surface, at its solvent side. These may have evolved at later stages to fine tune the complex tasks and intricate recognitions required for the decoding process. They also may prevent nonproductive interactions with the large subunit or the initiation factors.

The Decoding Center and Its Vicinity

The decoding center organizes mRNA and tRNA translocation and controls fidelity in codon–anticodon interactions (Green and Noller, 1997). It is located at the upper part of the body and the lower part of the head. Mapping the conserved nucleotides in the 16S RNA on our structure showed remarkable conservation around this region, in accord with the universality of the decoding

Table 1. MIRAS Phasing Statistics

Data Collection	Wative 1	Wative 2	Backsoak	Ir	IrG	Os	Ta_6Br_{12}
Reflections	2,186,910	327,448	725,465	154,875	218,049	82,258	99137
Unique reflections	206,724	133,199	122,788	45,748	71,096	25,593	48132
Completeness	94.7 (77.1)	80.5 (73.1)	86.4 (82.8)	91.3 (95.2)	69.3 (68.2)	70.4 (42.8)	56.1 (38.5)
Mean [I/sigma(I)]	21.9 (3.6)	12.3 (2.8)	14.5 (3.3)	11.5 (6.7)	10.7 (3.9)	12.8 (4.9)	10.5 (3.1)
R_{sym}	13.6 (44.1)	10.6 (29.4)	12.7 (34.7)	11.3 (34.2)	12.4 (24.8)	10.3 (46.3)	14.3 (33.2)
D_{min} (Å)	3.3	3.5	3.8	5.4	4.5	5.8	5.0
Phasing							
Sites	13[b]	10[b]	8[b]	14	4	15	5
R_{cullis} (centric)	—	0.67	0.60	0.64		0.87	0.82
R_{cullis} (acentric)[a]	—/0.80	0.76/0.66	0.72/0.56	0.80/0.83	0.75/0.66	0.87/0.63	0.88/—
PP (centric)	—	0.64	1.14	0.98	0.79	1.06	0.98
PP (acentric)[a]	—/0.65	0.70/0.94	1.22/0.75	1.21/0.85	0.96/1.13	1.32/0.73	1.13/—

PP: phasing power = <|Fh(calc)|>/<phase-integrated lack of closure. R_{cullis} = <phase-integrated lack of closure>/<|Fph − Fp|>. R_{cullis} and phasing power were obtained from SHARP. The compounds used for derivatization have been described in (Tocilj et al., 1999) except for Ir = sodium-Ir chloride. Additional minor heavy atoms used for phasing have been omitted from this table. The overall figure of merit (FOM) was 0.48 after MIRAS phasing with SHARP, and 0.78 after density modification with SOLOMON.

[a] Isomorphous/anomalous. Highest resolution bins are given in brackets.

[b] Number of W_{18} sites. Among them four were represented by individual atoms, the remaining sites by their spherically averaged form factor.

process. This region contains the upper part of H44, H45, the 3′ and 5′ ends of the 16S RNA, the switch helix (Lodmell and Dahlberg, 1997), H27, the central pseudoknot, H1/H2, and the stem loop of H18, and the main transverse head element, H34 (Figure 2).

The most prominent feature in the decoding center is the upper portion of H44 (also called the "penultimate stem"), which bends toward the neck. H44 forms much of the intersubunit contact in the assembled ribosome (Cate et al., 1999); its upper bulge—nucleotides 1492–1498 and their base pairs 1402–1408 (*E. coli* numbering)—form the A and P tRNA sites. The terminal helix, H45, packs between H44 and H24 and leads to the 3′ end of the 16S RNA. The 3′ segment is known to be highly flexible and contains the region that pairs with the trigger (Shine-Dalgarno) sequence in the mRNA, an interaction critical for initiation of protein synthesis. The switch helix can undergo changes in its base-pairing scheme; these may induce cooperative rearrangements that lead to movements of the platform, shoulder, and head (Gabashvili et al., 1999b). Thus, the global conformational state of the particle may be correlated with the base-pairing scheme of H27 (Lodmell and Dahlberg, 1997). We see in our map the conformation called 912–885 (*E. coli* numbering). As expected, the opening of the central pseudoknot is not observed, consistent with the importance of the integrity of the pseudoknot for the functionality of the ribosome (Poot et al., 1998).

H27 packs groove-to-groove with the upper end of H44, which is the target of amino-glycoside antibiotics. The structure of an RNA-paromomycin complex (Fourmy et al., 1998) indicates that the antibiotic causes the upper stem of H44 to bend toward H27; this bending may, in turn, induce a displacement of H27 toward S5. Such coordinated movement is permitted by the structure we see; it could explain the differences in streptomycin protection patterns observed in naked 16S rRNA and in complete 30S particles (Spickler et al., 1997), as well as the relations between mutations in H27 (Lodmell and Dahlberg, 1997) and the ribosomal ambiguity (*ram)* as well as the restrictive mutations.

The structural elements of the decoding center create between the head and the body an elongated, curved channel, which we assigned as the path of the mRNA. The loop of H18 is located near the entrance to this channel. In our structure it bends toward the decoding center, in agreement with crosslinking data (Powers and Noller, 1991; Bullard et al., 1998). Connecting between regions known to be mobile, and interacting with the incoming mRNA (Dontsova et al., 1992), this region may assume more than one conformation unless it is stabilized. Indeed, this region is somewhat less well defined in our map.

The positions of mRNA and tRNA in the decoding center were determined by reference to the structure (at 7.8 Å resolution) of a tRNA-70S complex (Cate et al., 1999). The entire penultimate stem is clearly defined in that structure, so we superposed this region onto our electron density map (Cate et al., 1999 and PDB entry 486D). Only a small shift was then needed to achieve a remarkable fit of the tRNA and mRNA codons with the geometry of the decoding center (Figure 3). The required shift, smaller than 6 Å, may be linked to the conformational rearrangements that the small subunit undergoes upon incorporation into the 70S particle or consequent to the binding of the mRNA/tRNA molecules. Alternatively, it may be due to the uncertainties of the limited resolution of the 70S map. We also found similarities between the shape of the decoding center seen in our structure and the contour of the corresponding part of the NMR structure of a 26-mer oligonucleotide of *E. coli* sequence (Fourmy et al., 1998) and with that adopted from it in modeling attempts (VanLoock et al., 1999).

An important conclusion, illustrated in Figure 3, is that the anticodon loops of the A and P site tRNAs and the codon segments of the mRNA do not contact any ribosomal proteins. The configuration of the 16S RNA therefore determines the precise arrangement of the interacting elements and enforces precision in codon–anticodon interactions. As seen at lower resolution in the structure of the 70S complex (Cate et al., 1999), the shape of the mRNA channel at the vicinity of the

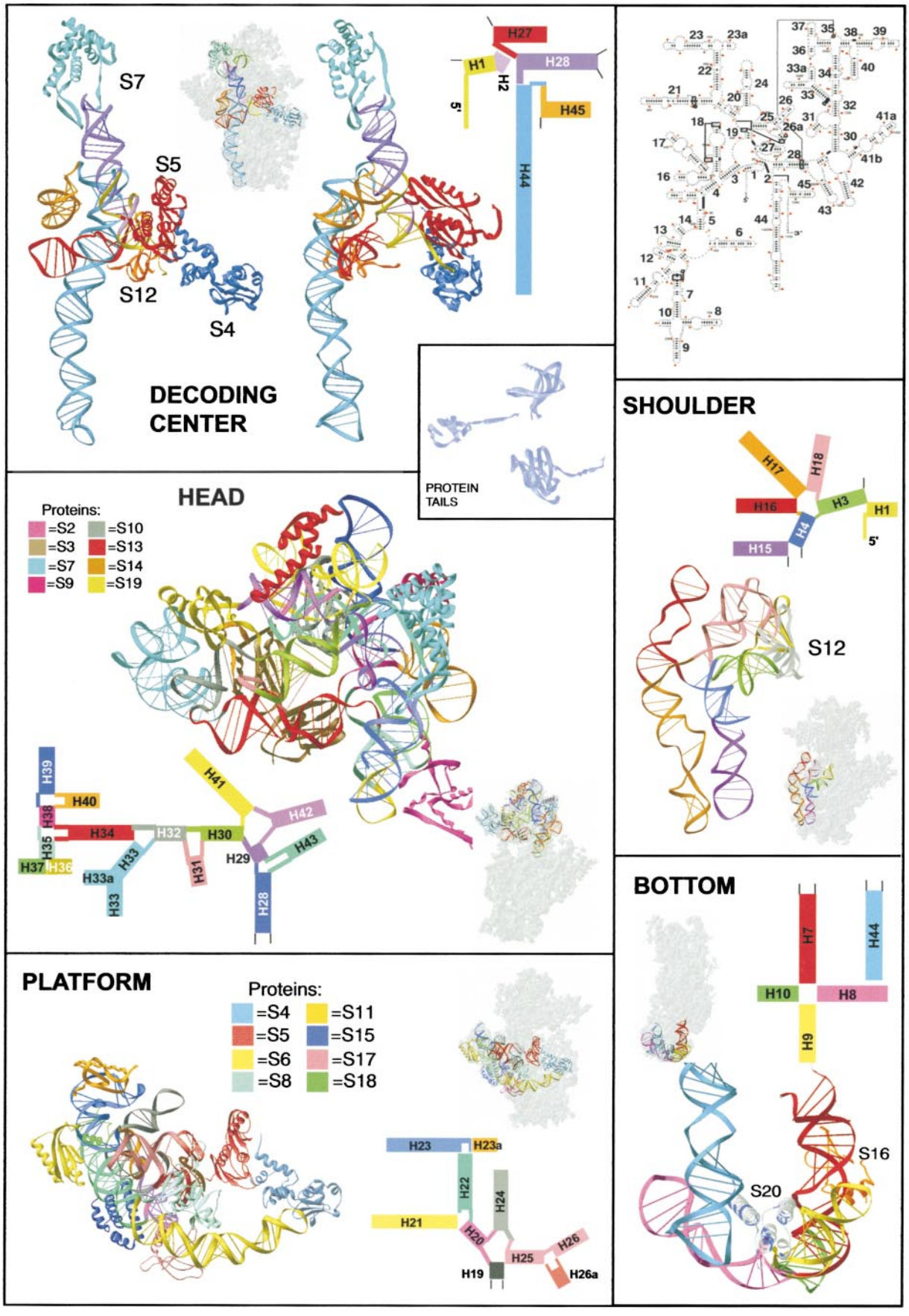
S7
S5
S12
S4
DECODING CENTER
H27
H28
H1
H2
5'
H45
H44
PROTEIN TAILS
SHOULDER
H17
H18
H16
H3
H1
H4
H15
5'
S12
HEAD
Proteins:
=S2
=S3
=S7
=S9
=S10
=S13
=S14
=S19
H39
H40
H38
H34
H32
H30
H41
H42
H35
H33
H31
H29
H43
H37
H36
H33a
H33
H28
BOTTOM
H7
H44
H10
H8
H9
S16
S20
PLATFORM
Proteins:
=S4
=S5
=S6
=S8
=S11
=S15
=S17
=S18
H23
H23a
H22
H24
H21
H20
H25
H26
H19
H26a

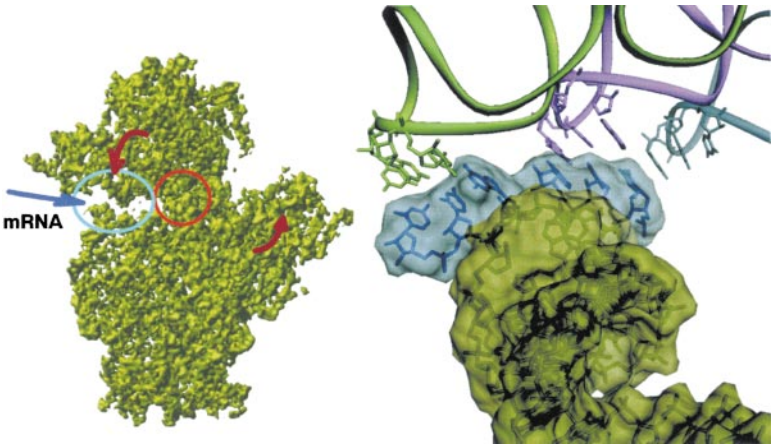

Figure 3. The Presumed mRNA Path

(Left) A surface representation of the subunit, viewed from the side of the 50S subunit. The latch is circled in cyan and the decoding center in red. The mRNA would enter the path in the approximate direction shown by the dark-blue arrow, pass through the aperture defined by the latch, and along the channel in the near face of the subunit. The brown curved arrows show the suggested global cooperative movements of the platform and the head, which facilitate the mRNA entrance, progression, and exit.

(Right) Enlarged image of the decoding center region, showing the positions of tRNA anticodon stem loops and mRNA codons, using the superposition of tRNA and mRNA from the model of Cate et al., 1999, as described in the text. The uppermost bulge of H44 is shown in olive, two codons of mRNA in blue, and the anticodon bases of the tRNA molecules in green (A site), magenta (P site) and gray (E site). The right side of the figure was made with DINO (Philippsen, 2000). The contour level is 1.1 standard deviations.

decoding center dictates formation of two successive kinks along the mRNA, allowing two tRNA molecules to be bound simultaneously and to be translocated with the mRNA chain, thus guaranteeing processivity.

Inspection of the P and E sites revealed a noteworthy example of protein-RNA mimicry. The P site tRNA interacts with helix H30, and a similar contour is contributed by protein S7 for its interaction with the E site tRNA. If the primitive ribosome contained only RNA, and the biosynthetic process required only two tRNA molecules, protein S7 may have evolved as a refinement to define the third tRNA position more precisely and to assist in the post translocational ejection of the E site tRNA.

A Latch at the Entrance of the mRNA Channel

The positions of tRNA and messenger-RNA, as determined by the superposition described above, show that mRNA must enter the channel through a pore created by a noncovalent connection between the head and body (Figure 3). To form this contact, H33/H34 project from the rim of the nose, and H16/H18 project from the shoulder, in accord with results from hydroxyl-radical cleavage experiments (Newcomb and Noller, 1999). This interaction is not seen in structures of nonactivated small subunits determined by cryo-EM (Gabashvili et al., 1999a; Harms et al., 1999) or X-ray crystallography (Clemons et al., 1999), but it is present in functional complexes of 70S ribosomes analyzed by either method (Stark et al., 1997, 2000; Cate et al., 1999; Frank and Agrawal, 2000). Closure of this "latch" is clearly due to the stabilization of the active conformation of the small subunit in our crystals. Comparisons between the present and previously determined 30S structures suggest that latch closure results from an intricate network of conformational rearrangements, involving H27, H28, and H34. These observations are in excellent agreement with the findings that opening and closing of the mRNA channel relate to the base-pairing states of the accuracy switch (Lodmell and Dahlberg, 1997; Gabashvili et al., 1999b), which depends in turn on the activation state of the ribosome (Frank and Agrawal, 2000). They are also in remarkable accord with recent targeting experiments in which the region participating in the formation of the latch was protected in activated particles and exposed in nonactivated subunits (Muth et al., 2000), suggesting that changes in the latch elements are linked to rearrangements of H34 (Stark et al., 2000) and may explain frame-shifting caused by pseudoknots in the mRNA (Kim et al., 1999). We propose that closing of the latch provides a geometry that guarantees processivity

Figure 2. Selected Structural Elements within the Small Ribosomal Subunit

Each element is shown as ribbon representations of the RNA segments and the proteins that contribute to it, together with the superposition of the element on the outline of the small subunit (gray). For each region the RNA secondary-structural elements are included, color coded to match.

The decoding center: The view on the left corresponds to rotating the object in Figure 1 by about 45° around the vertical axis (counterclockwise when seen from above), so that the platform moves toward the viewer and the nose moves away. In this view, mRNA would enter from the right rear and exit from the left front. The view on the right is roughly perpendicular to the right one.

The head: The view is about 180° from Figure 1, that is, from the side of the 50S subunit in an assembled ribosome. Note, for example, that the nose now points to the left.

The shoulder is viewed from the 50S subunit side, as shown in (B).

The bottom of the particle is seen at about 90° to the viewpoint of Fig. 1, as if from the left. That is, in an assembled ribosome, the 50S subunit would be on the left in this figure and the solvent on the right.

The platform is viewed from the solvent side, as in Figure 1. Helices H21–23 form the framework of the platform, on the solvent-facing side of the body.

Insets: (Top right) The secondary-structure diagram of the 16S RNA from *T. thermophilus* (Gutell et al., 1999), with helix numbering according to Mueller and Brimacombe, 1997.

(Middle) Within the "decoding center": the folds of proteins S5, S12, and S17 (counterclockwise, starting on top), as examples for long protruding arms.

and ensures maximum fidelity. If conformational changes in the platform and head drive translocation of mRNA-tRNA complexes, then the latch may provide directionality and prevent dissociation.

The Body

The body of the 30S subunit has a relatively compact lower part ("foot") and a wider and more flexible upper region, comprising the platform, the shoulder, and the decoding-center cleft. The foot appears to serve as an anchor to control the inclination and orientation of the main features in the intersubunit interface and in the decoding center. It contains H6-H11 and protein S20 (Figure 2). H7 runs longitudinally, parallel to H44, and branches into H8, which defines the lower boundary of the particle. H9 has extensive groove–groove contacts with H7, with its tetraloop facing outward. H7 connects with H11, which is sandwiched between H7 and H44. Helices H6–H11 and the distal end of H44 are clamped together by a highly α-helical protein, identified as S20, based on immunoelectron microscopy (Schwedler et al., 1993) and directed hydroxyl radical probing (Culver and Noller, 1998). Its sequence (to be published) shows periodically distributed lysines and arginines that form a positively charged surface to contact the sugar-phosphate backbone of the RNA. These characteristics suggest that S20 recognizes RNA structure rather than sequence, and indeed, neither the distal end of H44 nor the segment H8-H9 has a highly conserved nucleotide sequence. Despite its remote location, S20 contributes significantly to the decoding process: mutants lacking S20 exhibit misreading, temperature sensitivity, reduced capacity for intersubunit association, and impaired P site codon–anticodon interaction (Gotz et al., 1990; Ryden-Aulin et al., 1993). S20 must therefore function in part by maintaining the correct orientation of H44.

The effects of mutations in S20 demonstrate an important consequence of the striking architecture of the body. In this construction three major longitudinal elements, H44, H16/H17, and H7, act as structural pillars that extend for over 110 Å. They can therefore not only stabilize the body but also transmit conformational changes and displacements over a very long distance.

The platform (Figure 2) contributes to P site tRNA binding and is known to shift when subunits associate (Gabashvili et al., 1999b). It contains H20–H24 and proteins S6, S8, S11, S15, and S18 (Figure 2). Its central substructure, containing all proteins mentioned above apart from S11, has been studied at high resolution (Agalarov et al., 2000; Nikulin et al., 2000) and part of it has been assigned in crystallographic studies of the entire subunit at low resolution (Clemons et al., 1999). In essence, all four independently determined structures are closely related. However, we observed differences in the relative locations of some of the platform's components, when comparing the structures of our activated particle and of the nonactivated one (Clemons et al., 1999). The coaxial stack, H23 and H22, define one arm of the broad, L-shaped domain, and H21, which projects toward the shoulder, defines the other. Groove-to-groove contacts between H23 and H24 anchor the base of the platform; H25 and H26, mutually perpendicular, form a binding surface for S8. Contacts between H22 and H25 further tighten the core of the structure. The platform and the shoulder are connected by a protein-rich belt, which contains S4, S5, and S8 (Figure 2).

The shoulder contains two major, longitudinal rods, made of H15/H18 and H16/H17 (Figure 2). Their side-by-side interactions appear to form the backbone of the entire body. The packing of the mutually perpendicular H3 and H4 creates a highly compact fold in the five-way junction, H3/H4/H16/H17/H18, which is connected to the central pseudoknot through H3. The loops of H16 and H18 form one side of the latch, as described above.

The putative path taken by the messenger is located in this region. The components likely to interact with mRNA as it threads its way from the latch into the channel include the loop of H18 and proteins S3, S4, S5, and S12. S4, S5, and S12 (Baranov et al., 1999) probably assist the directionality of the decoding process and the accuracy in translation, as it has been observed that *ram* (ribosomal ambiguity) mutations in S4 and S5 cause misreading and the restrictive mutations in S12 enhance the fidelity (van Acken, 1975; Wittmann-Liebold and Greuer, 1978; Alksne et al., 1993). The anti-Shine-Dalgarno sequence, which is located at the 3′ end of the 16S RNA hybridizes with the incoming 5′ end of the mRNA. By use of an mRNA analog (a cDNA oligomer of 22 nucleotides) to which heavy atom markers had been bound prior to hybridization, the 3′ end of the 16S RNA could be located near H45 on the upper side of the platform, in the vicinity of S11 and the binding site of initiation factor IF3 (Tocilj et al., 1999; Auerbach et al., 2000; Bashan et al., 2000; further details to be published).

The Head and Neck

The head (Figure 2) contains most of the 3′ region of the 16S RNA (but not, of course, the last two helices, H44 and H45). It interacts with mRNA, elongation factor G, tRNA, and several antibiotics (Dontsova et al., 1992; Wilson and Noller, 1998; Stark et al., 2000). The proteins of the head appear to help stabilize its fold, which contains short helices and several multihelix junctions with complicated architecture. The head proteins fall mainly, but not exclusively, into two groups, on opposite sides of the domain, as suggested by early immunoelectron microscopy (Oakes et al., 1986; Stöffler and Stöffler-Meilicke, 1986). The crest of the head contains H41 and H42; the nose includes H33 and H33a; the side opposite the nose contains the stacked helices H35/H36/H38/H39. Helices H29, H30, and H32 wrap around the head and form a link to it. This unusual RNA arrangement creates an oval-shaped protein pocket. The three-way junction loop connecting H28, H29, and H43 is organized as a highly conserved, modular RNA motif (Leontis and Westhof, 1998), with similarity to loop E (Szewczak et al., 1993). This junction loop contributes to the P site for tRNA (Leontis and Westhof, 1998). Protein S7, which has been specifically crosslinked to tRNA and mRNA analogs (Dontsova et al., 1991), binds to this loop. In our model, S7 lies closer to the E site tRNA than to the P site tRNA, but its effects on stability of the fold of the 16S RNA could propagate to the entire decoding center.

H28 is the only covalent connection from the body to the head. The base-pair mismatches within it cause some structural deviations from strict A-form geometry; it is possible that these deviations are related to the postulated role of the neck as a hinge for global head motions. Variability in the shape of the head, as seen by cryo-EM (Frank et al., 1995; Stark et al., 1995; Gabashvili et al., 1999a; Harms et al., 1999) and by

X-ray crystallography (Clemons et al., 1999), shows that adjustments and conformational changes may occur within the domain, in addition to the suggested hinge motions about the neck. Conformational changes of either type may take place even within crystals, and the head may be stabilized by association with the large subunit or by nonribosomal elements, such as the W clusters in our crystals (Tocilj et al., 1999). Indeed, the apparent variability in the orientation of the head is likely to be coupled to the movement of the platform, which is known to shift upward upon subunit interaction, IF3 binding or heat activation (Gabashvili et al., 1999b, 2000). Global shifts of around 5–6 Å of the platform were also observed by superposition of the coordinates of the penultimate helix as determined for the nonactivated small subunit at 5.5 Å (Clemons et al., 1999 and PDB IQD7) on the structure of the functionally activated particle presented here.

Conclusions

The picture of the ribosomal small subunit that emerges from our analysis is one of a precisely engineered machine, with shifts coupled over long as well as short distances to create a defined sequence of events at the decoding center. Thus, mutational changes at the foot of the subunit can affect the accuracy of translation, because long helices link the foot with the center of the subunit, and motions of the head may open and close the mRNA latch. The head and platform motions may be coupled to the state of the switch helix, H27. The decoding center itself is formed exclusively of RNA, and even the closest proteins, S12 and S7, seem to serve ancillary functions such as stabilizing required conformation and assisting the translocation. The kinks in mRNA are enforced by the shape of the decoding site, and the positions of the anticodons of A and P site tRNAs are determined by cavities bounded by polynucleotide. A more extensive description of the dynamics of mRNA association and translocation will clearly require many additional structures, among them of antibiotics-bound particles, such as edeine. The present results provide a structural framework for better understanding the mechanisms associated with the decoding of the genetic information. They make the first complete bridge from the language of gross anatomy to the language of chemistry at close to atomic resolution.

Experimental Procedures

Crystals

Crystals in space group P41212 (a = b = 406.3 Å; c = 173.1 Å), were grown from heat-activated (Zamir et al., 1971) 30S subunit from T. *thermophilus,* as described in (Tocilj et al., 1999). Postcrystallization heat activation, followed by stabilization by $(K_6(P_2W_{18})O_{62})14H_2O$ (called here W18), was performed to increase the homogeneity of the activated form within the crystals, yielding a dramatic increase in the resolution. The functionally active conformation of the 30S subunits within these crystals (called here Wative) was confirmed since they were found to be isomorphous with crystals containing substrate analogs, the 5′ end of mRNA (Tocilj et al., 1999; Auerbach et al., 2000) or IF3, one of the factors that together with 30S and mRNA participates in the ribosomal initiation complex. Cocrystals of 30S with either the initiation factor IF3 or the antibiotic edeine were obtained under the same conditions. When treated by W18, they yielded diffraction of comparable resolution (3.3–3.6 Å).

Heavy-atom derivatives were prepared as described previously (Tocilj et al., 1999). The crystals contain a single 30S particle and seven W18 clusters in an asymmetric unit. The clusters stabilize and rigidify the particle (Tocilj et al., 1999). X-ray diffraction data were collected at 95K, using bright synchrotron radiation. The data were recorded on image-plate (MAR 345) or CCD (Mar, Quantum 4, or APS2) and processed with DENZO (Otwinowski and Minor, 1997). They were reduced either with SCALEPACK (Otwinowski and Minor, 1997) or with the CCP4 package (Bailey, 1994).

MIRAS Phasing

MIRAS phasing was carried out as summarized in Table 1. The W18 sites were obtained from difference Patterson and residual maps. Minor sites and sites of the smaller heavy-atom compounds were obtained form difference Fourier and residual maps. Phase refinement was performed using SHARP (de la Fortelle and Bricogne, 1997), by sequential addition of the derivatives after prerefinement. Individual W atoms of the well-ordered W18 clusters were used for phasing beyond 4.5 Å; otherwise, the tungsten clusters were represented by their spherically averaged form-factor.

Density Modification

Density modification was carried out using SOLOMON (Abrahams and Leslie, 1996). To remove potential bias of W18, the density modification procedure was altered to include gradually the low-resolution terms.

Model

The model was built using the sequence of the 16S RNA and the proteins from *T. thermophilus* (except for protein S16, for which we exploited the sequence of *Bacillus subtilis* since that of *T. thermophilus* was not available). The program O (Jones and Kjeldgaard, 1997) was used for map interpretation. Initially the map was interpreted at 3.8 Å. At that stage the map was sufficiently clear that the backbone phosphates could be positioned unambiguously for most of the RNA chain. Density for the bases was present, but individual bases were hardly separated. The RNA chain was traced by following features in the map, while maintaining acceptable bond lengths and angles. Subsequently we consulted the primary sequence and the secondary-structure diagrams of the 16S RNA (Gutell et al., 1999) to confirm our interpretation. In most cases, no significant discrepancies were detected. The few disagreements are associated mainly with multiple junctions. One example is the three-way junction of H28/H29/H43, which does not show the triplet formation but instead contains an E loop motif, as suggested by (Leontis and Westhof, 1998). Where coordinates for individual proteins were available, they were introduced as rigid bodies, and rebuilt as needed. We also consulted the structures of the RNA-protein complexes that became available after our 3.8 Å map was traced. The spatial arrangement of the rRNA chains was found to be in reasonable agreement with most of the independently derived biochemical and biophysical data.

The current 3.3 Å map shows a large number of well-resolved individual bases and protein side chains (Figure 1). The folds of the proteins that had not been determined by NMR or X-ray crystallography could be assigned directly from the map. We also could trace most of the previously undetermined parts of those proteins that have been analyzed as isolated entities by crystallography or NMR.

An example for our assignment strategy at its initial stage is given below. Apart from S7 and S19, the structures of the head proteins have not been determined independently, but density for the majority was readily detected even in our 3.8 Å map. The α-helical region above S7 was assigned to S9, exploiting crosslinking data (Baranov et al., 1999). S13, containing three parallel α helices, was located at the crest of the head in the vicinity of S19. This assignment relied on the pairing of S13 and S19 (Pohl and Wittmann-Liebold, 1988), on immuno-EM results (Montesano-Roditis et al., 1993), and on the position of a heavy-atom marker bound to an exposed cysteine of S13, prior to the crystallization (Weinstein et al., 1999). The map shows features of an S6 motif near H39; as S10 cross links to RNA components of this region and as its sequence predicts an S6-like structure, we assigned S10 to this density. S2 was identified close to H35-H37, in accord with biochemical data (Powers et al., 1988). Once the resolution improved, several regions became clearer and adjustments could be made.

Refinement with CNS (Brünger et al., 1998) and REFMAC (Murshudov et al., 1999) are in progress. An initial rigid-body refinement with bulk solvent correction yielded R_{free} of 30.5%. The correctness of the fit was assessed by using OMIT procedures, inspecting $2F_o$-F_c sigma$_a$ weighted map (Bailey, 1994).

Acknowledgments

Raz Zarivach contributed significantly to the tracing, and Joerg Harms to the assignments. We thank S. Harrison and W. Traub for critical review of the manuscript, M. Wilchek for indispensable advice, M. Pope for heavy-atom compounds, R. Brimacombe and H. Stark for fruitful discussions. We thank R. Albrecht, T. Auerbach, H. Avila, W.S. Bennett, H. Burmeister, D. Choli, C. Glotz, H.A.S. Hansen, R. Kafri, K. Knaack, M. Laschever, S. Meier, J. Muessig, M. Pioletti, M. Peretz, C. Radzwill, I. Sagi, B. Schmidt, A. Vieweger, and S. Weinstein for contributing to different stages of these studies. These studies could not be performed without the cooperation of the staff of the synchrotron radiation facilities at EMBL & MPG beam lines at DESY; ID2 and ID14/2 and 4 at EMBL and ESRF; ID19/APS/ANL and F1/CHESS. Support was provided by the Max-Planck Society, the US National Institutes of Health (GM34360), the German Ministry for Science and Technology (Bundesministerium für Bildung, Wissenschaft, Forschung und Technologie Grant 05-641EA), and the Kimmelman Center for Macromolecular Assembly at the Weizmann Institute. A. Y. holds the Martin S. Kimmel Professorial Chair.

Received June 23, 2000; revised July 31, 2000.

References

Abrahams, J.P., and Leslie, A.G.W. (1996). Methods used in the structure determination of bovine mitochondrial F-1 ATPase. Acta Crystallogr. Sect. D Biol. Crystallogr. *52*, 30–42.

Agalarov, S.C., Sridhar Prasad, G., Funke, P.M., Stout, C.D., and Williamson, J.R. (2000). Structure of the S15, S6, S18-rRNA complex: assembly of the 30S ribosome central domain. Science *288*, 107–113.

Alksne, L.E., Anthony, R.A., Liebman, S.W., and Warner, J.R. (1993). An accuracy center in the ribosome conserved over 2 billion years. Proc. Natl. Acad. Sci. USA *90*, 9538–9541.

Arad, T., Piefke, J., Weinstein, S., Gewitz, H.S., Yonath, A., and Wittmann, H.G. (1987). Three-dimensional image reconstruction from ordered arrays of 70S ribosomes. Biochimie *69*, 1001–1006.

Auerbach, T., Pioletti, M., Avila, H., Anagnostopoulos, K., Weinstein, S., Franceschi, F., and Yonath, A. (2000). Genetic and biochemical manipulations of the small ribosomal subunit from *Thermus thermophilus* HB8. J. Biomol. Struct. Dyn. *17*, 617–628.

Bailey, S. (1994). The Ccp4 suite—programs for protein crystallography. Acta Crystallogr. Sect. D Biol. Crystallogr. *50*, 760–763.

Ban, N., Nissen, P., Hansen, J., Capel, M., Moore, P.B., and Steitz, T.A. (1999). Placement of protein and RNA structures into a 5 Å-resolution map of the 50S ribosomal subunit. Nature *400*, 841–847.

Baranov, P.V., Kubarenko, A.V., Gurvich, O.L., Shamolina, T.A., and Brimacombe, R. (1999). The database of ribosomal cross-links: an update. Nucleic Acids Res. *27*, 184–185.

Bashan, A., Pioletti, M., Bartels, H., Janell, D., Schlünzen, F., Glühmann, M., Levin, I., Harms, J., Hansen, H.A.S., Tocilj, A., et al. (2000). Identification of selected ribosomal components in crystallographic maps of prokaryotic ribosomal subunits at medium resolution. In The Ribosome: Structure, Function, Antibiotics and Cellular Interactions, R. Garrett, S. Douthwaite, A. Liljas, A. Matheson, P. Moore, and H. Noller, eds. (Washington D.C.: ASM Press), pp. 21–33.

Brünger, A.T., Adams, P.D., Clore, G.M., DeLano, W.L., Gros, P., Grosse-Kunstleve, R.W., Jiang, J.S., Kuszewski, J., Nilges, M., Pannu, N.S., Read, R.J., Rice, L.M., Simonson, T., and Warren, G.L. (1998). Crystallography & NMR system: a new software suite for macromolecular structure determination. Acta Crystallogr. Sect. D Biol. Crystallogr. *54*, 905–921.

Bullard, J.M., van Waes, M.A., Bucklin, D.J., Rice, M.J., and Hill, W.E. (1998). Regions of 16S ribosomal RNA proximal to transfer RNA bound at the P-site of *Escherichia coli* ribosomes. Biochemistry *37*, 1350–1356.

Carson, M. (1997). Ribbons. Methods Enzymol. *277*, 493–505.

Cate, J.H., Yusupov, M.M., Yusupova, G.Z., Earnest, T.N., and Noller, H.F. (1999). X-ray crystal structures of 70S ribosome functional complexes. Science *285*, 2095–2104.

Choli, T., Franceschi, F., Yonath, A., and Wittmann-Liebold, B. (1993). Isolation and characterization of a new ribosomal protein from the thermophilic eubacteria, *Thermus thermophilus*, *Thermus aquaticus* and *Thermus flavus*. Biol. Chem. Hoppe-Seyler *346*, 377–383.

Clemons, W.M., Jr., May, J.L., Wimberly, B.T., McCutcheon, J.P., Capel, M.S., and Ramakrishnan, V. (1999). Structure of a bacterial 30S ribosomal subunit at 5.5 A resolution. Nature *400*, 833–840.

Conn, G.L., Draper, D.E., Lattman, E.E., and Gittis, A.G. (1999). Crystal structure of a conserved ribosomal protein-RNA complex. Science *284*, 1171–1174.

Culver, G.M., and Noller, H.F. (1998). Directed hydroxyl radical probing of 16S ribosomal RNA in ribosomes containing Fe(II) tethered to ribosomal protein S20. RNA *4*, 1471–1480.

de la Fortelle, E., and Bricogne, G. (1997). Maximum-likelihood heavy-atom parameter refinement for multiple isomorphous replacement and multiwavelength anomalous diffraction methods. Macromol. Crystallogr. A *276*, 472–494.

Dontsova, O., Kopylov, A., and Brimacombe, R. (1991). The location of messenger-RNA in the ribosomal 30S initiation complex—site-directed cross-linking of messenger-RNA analogs carrying several photo-reactive labels simultaneously on either side of the AUG start codon. EMBO J. *10*, 2613–2620.

Dontsova, O., Dokudovskaya, S., Kopylov, A., Bogdanov, A., Rinke-Appel, J., Junke, N., and Brimacombe, R. (1992). Three widely separated positions in the 16S-RNA lie in or close to the ribosomal decoding region—a site-directed cross-linking study with messenger-RNA analogs. EMBO J. *11*, 3105–3116.

Fourmy, D., Yoshizawa, S., and Puglisi, J.D. (1998). Paromomycin binding induces a local conformational change in the A-site of 16 S rRNA. J. Mol. Biol. *277*, 333–345.

Frank, J., and Agrawal, R.K. (2000). A ratchet-like inter-subunit reorganization of the ribosome during translocation. Nature *406*, 318–322.

Frank, J., Zhu, J., Penczek, P., Li, Y.H., Srivastava, S., Verschoor, A., Radermacher, M., Grassucci, R., Lata, R.K., and Agrawal, R.K. (1995). A model of protein synthesis based on cryo-electron microscopy of the *E. coli* ribosome. Nature *376*, 441–444.

Gabashvili, I.S., Agrawal, R.K., Grassucci, R., and Frank, J. (1999a). Structure and structural variations of the *Escherichia coli* 30S ribosomal subunit as revealed by three-dimensional cryo-electron microscopy. J. Mol. Biol. *286*, 1285–1291.

Gabashvili, I.S., Agrawal, R.K., Grassucci, R., Squires, C.L., Dahlberg, A.E., and Frank, J. (1999b). Major rearrangements in the 70S ribosomal 3D structure caused by a conformational switch in 16S ribosomal RNA. EMBO J. *18*, 6501–6507.

Gabashvili, I.S., Agrawal, R.K., Spahn, C.M., Grassucci, R.A., Svergun, D.I., Frank, J., and Penczek, P. (2000). Solution structure of the *E. coli* 70S ribosome at 11.5 A resolution. Cell *100*, 537–549.

Gotz, F., Dabbs, E.R., and Gualerzi, C.O. (1990). *Escherichia coli* 30S mutants lacking protein S20 are defective in translation initiation. Biochim. Biophys. Acta *1050*, 93–97.

Green, R., and Noller, H.F. (1997). Ribosomes and translation. Annu. Rev. Biochem. *66*, 679–716.

Gutell, R.R., Subashchandran, S., Schnare, M., Du, Y., Lin, N., Madabusi, L., Muller, K., Pande, N., Yu, N., Shang, Z., Date, S., Konings, D., Schweiker, V., Weiser, B., and Cannone, J.J. (1999). Comparative sequence analysis and the prediction of RNA structure, and the Web. http://www.rna.icmb.utexas.edu/.

Harms, J., Tocilj, A., Levin, I., Agmon, I., Stark, H., Kölln, I., van Heel, M., Cuff, M., Schlünzen, F., Bashan, A., Franceschi, F., and Yonath, A. (1999). Elucidating the medium-resolution structure of ribosomal particles: an interplay between electron cryo-microscopy and X-ray crystallography. Structure Fold. Des. *7*, 931–941.

Helgstrand, M., Rak, A.V., Allard, P., Davydova, N., Garber, M.B., and Hard, T. (1999). Solution structure of the ribosomal protein S19 from *Thermus thermophilus*. J. Mol. Biol. *292*, 1071–1081.

Jones, T.A., and Kjeldgaard, M. (1997). Electron-density map interpretation. Methods Enzymol. *277*, 173–208.

Kim, Y.G., Su, L., Maas, S., O'Neill, A., and Rich, A. (1999). Specific mutations in a viral RNA pseudoknot drastically change ribosomal frameshifting efficiency. Proc. Natl. Acad. Sci. USA *96*, 14234–14239.

Leontis, N.B., and Westhof, E. (1998). A common motif organizes the structure of multi-helix loops in 16 S and 23 S ribosomal RNAs. J. Mol. Biol. *283*, 571–583.

Lodmell, J.S., and Dahlberg, A.E. (1997). A conformational switch in *Escherichia coli* 16S ribosomal RNA during decoding of messenger RNA. Science *277*, 1262–1267.

Luger, K., Mader, A.W., Richmond, R.K., Sargent, D.F., and Richmond, T.J. (1997). Crystal structure of the nucleosome core particle at 2.8 Å resolution. Nature *389*, 251–260.

Montesano-Roditis, L., McWilliams, R., Glitz, D.G., Olah, T.V., Perrault, A.R., and Cooperman, B.S. (1993). Placement of dinitrophenyl-modified ribosomal proteins in totally reconstituted *Escherichia coli* 30S subunits: Localization of proteins S6, S13, S16, and S18 by immune electron microscopy. J. Biol. Chem. *268*, 19701–19709.

Mueller, F., and Brimacombe, R. (1997). A new model for the three-dimensional folding of *Escherichia coli* 16S ribosomal RNA. I. Fitting the RNA to a 3D electron microscopic map at 20 Å. J. Mol. Biol. *271*, 524–544.

Mueller, F., Stark, H., vanHeel, M., Rinke-Appel, J., and Brimacombe, R. (1997). A new model for the three-dimensional folding of *Escherichia coli* 16 S ribosomal RNA. III. The topography of the functional centre. J. Mol. Biol. *271*, 566–587.

Murshudov, G.N., Levedev, A., Vagin, A.A., Wilson, K.S., and Dodson, E.J. (1999). Efficient anisotropic refinement of macromolecular structures using FFT. Acta Crystallogr. Sect. D Biol. Crystallogr. *55*, 247–255.

Murzina, N.V., Vorozheykina, D.P., and Matvienko, N.I. (1988). Nucleotide sequence of *Thermus thermophilus* HB8 gene coding 16S ribosomal-RNA. Nucleic Acids Res. *16*, 8172–8172.

Muth, G.W., Hennelly, S.P., and Hill, W.E. (2000). Using a targeted chemical nuclease to elucidate conformational changes in the *E. coli* 30S ribosomal subunit. Biochemistry *34*, 4068–4074.

Newcomb, L.F., and Noller, H.F. (1999). Directed hydroxyl radical probing of 16S rRNA in the ribosome: spatial proximity of RNA elements of the 3′ and 5′ domains. RNA *5*, 849–855.

Nikulin, A., Serganov, A., Ennifar, E., Tishchenko, S., Nevskaya, N., Shepard, W., Portier, C., Garber, M., Ehresmann, B., Ehresmann, C., Nikonov, S., and Dumas, P. (2000). Crystal structure of the S15-rRNA complex. Nat. Struct. Biol. *7*, 273–277.

Oakes, M., Henderson, E., Scheinman, A., Clark, M., and Lake, J.A. (1986). Ribosome structure, function and evolution: mapping ribosomal RNA, proteins, and functional sites in three dimensions. In Structure, Function and Genetics of Ribosomes, B. Hardesty and G. Kramer, eds. (Berlin: Springer Verlag), pp. 47–67.

Otwinowski, Z., and Minor, W. (1997). Processing of X-ray diffraction data collected in oscillation mode. Macromol. Crystallogr. A *276*, 307–326.

Philippsen, A. (2000). DINO: Visualizing Structural Biology. http://www.bioz.unibas.ch/∼xray/dino.

Pohl, T., and Wittmann-Liebold, B. (1988). Identification of a cross-link in the *Escherichia coli* ribosomal protein pair S13–S19 at the amino acid level. J. Biol. Chem. *263*, 4293–4301.

Poot, R.A., van den Worm, S.H., Pleij, C.W.A., and van Duin, J. (1998). Base complementarity in helix 2 of the central pseudoknot in 16S rRNA is essential for ribosome functioning. Nucleic Acids Res. *26*, 549–553.

Powers, T., and Noller, H.F. (1991). A functional pseudoknot in 16S ribosomal-RNA. EMBO J. *10*, 2203–2214.

Powers, T., Stern, S., Changchien, L.M., and Noller, H.F. (1988). Probing the assembly of the 3′ major domain of 16 S rRNA interactions involving ribosomal proteins S2, S3, S10, S13 and S14. J. Mol. Biol. *201*, 697–716.

Ramakrishnan, V., and White, S.W. (1998). Ribosomal protein structures: insights into the architecture, maschinery and evolution of the ribosome. Trends Biochem. Sci. *23*, 208–212.

Ryden-Aulin, M., Shaoping, Z., Kylsten, P., and Isaksson, L.A. (1993). Ribosome activity and modification of 16S RNA are influenced by deletion of ribosomal protein S20. Mol. Microbiol. *7*, 983–992.

Schwedler, G., Albrecht-Ehrlich, R., and Rak, K.H. (1993). Immunoelectron microscopic localization of ribosomal proteins BS8, BS9, BS20, BL3 and BL21 on the surface of 30S and 50S subunits from *Bacillus stearothermophilus*. Eur. J. Biochem. *217*, 361–369.

Spickler, C., Brunelle, M.N., and Brakier-Gingras, L. (1997). Streptomycin binds to the decoding center of 16 S ribosomal RNA. J. Mol. Biol. *273*, 586–599.

Stark, H., Mueller, F., Orlova, E.V., Schatz, M., Dube, P., Erdemir, T., Zemlin, F., Brimacombe, R., and Heel, M. (1995). The 70S *Escherichia coli* ribosome at 23 Å resolution: fitting the ribosomal RNA. Structure *3*, 815–821.

Stark, H., Rodnina, M.V., Rinke-Appel, J., Brimacombe, R., Wintermeyer, W., and van Heel, M. (1997). Visualization of elongation factor Tu on the *Escherichia coli* ribosome. Nature *389*, 403–406.

Stark, H., Rodnina, M.V., Wieden, H.J., van Heel, M., and Wintermeyer, W. (2000). Large-scale movement of elongation factor G and extensive conformational change of the ribosome during translocation. Cell *100*, 301–309.

Stöffler, G., and Stöffler-Meilicke, M. (1986). Immuno electron microscopy on *Escherichia coli* ribosomes. In Structure, Function and Genetics of Ribosomes, B. Hardesty and G. Kramer, eds. (Berlin: Springer Verlag), pp. 28–46.

Szewczak, A.A., Moore, P.B., Chang, Y.L., and Wool, I.G. (1993). The conformation of the sarcin/ricin loop from 28S ribosomal RNA. Proc. Natl. Acad. Sci. USA *90*, 9581–9585.

Tocilj, A., Schlünzen, F., Janell, D., Glühmann, M., Hansen, H.A., Harms, J., Bashan, A., Bartels, H., Agmon, I., Franceschi, F., and Yonath, A. (1999). The small ribosomal subunit from *Thermus thermophilus* at 4.5 A resolution: pattern fittings and the identification of a functional site. Proc. Natl. Acad. Sci. USA *96*, 14252–14257.

Tsiboli, P., Herfurth, E., and Choli, T. (1994). Purification and characterization of the 30S ribosomal proteins from the bacterium *Thermus thermophilus*. Eur. J. Biochem. *226*, 169–177.

van Acken, U. (1975). Protein chemical studies on ribosomal proteins S4 and S12 from ram (ribosomal ambiguity) mutants of *Escherichia coli*. Mol. Gen. Genet. *140*, 61–68.

VanLoock, M.S., Easterwood, T.R., and Harvey, S.C. (1999). Major groove binding of the tRNA/mRNA complex to the 16 S ribosomal RNA decoding site. J. Mol. Biol. *285*, 2069–2078.

Weinstein, S., Jahn, W., Glotz, C., Schlünzen, F., Levin, I., Janell, D., Harms, J., Kölln, I., Hansen, H.A.S., Glühmann, M., et al. (1999). Metal compounds as tools for the construction and the interpretation of medium-resolution maps of ribosomal particles. J. Struct. Biol. *127*, 141–151.

Wilson, K.S., and Noller, H.F. (1998). Mapping the position of translational elongation factor EF-G in the ribosome by directed hydroxyl radical probing. Cell *92*, 131–139.

Wimberly, B.T., Guymon, R., McCutcheon, J.P., White, S.W., and Ramakrishnan, V. (1999). A detailed view of a ribosomal active site: the structure of the L11-RNA complex. Cell *97*, 491–502.

Wittmann-Liebold, B., and Greuer, B. (1978). The primary structure of protein S5 from the small subunit of the *Escherichia coli* ribosome. FEBS Lett. *95*, 91–98.

Zamir, A., Miskin, R., and Elson, D. (1971). Inactivation and reactivation of ribosomal subunits: amino acyl transfer RNA binding activity of the 30S subunit from *Escherichia coli*. J. Mol. Biol. *60*, 347–364.

Protein Data Bank ID Code

The coordinates reported in this paper have been deposited in the Protein Data Bank under ID code 1FKA.